ORIGINAL RESEARCH

Single-Photon Emission Computed Tomography/Computed Tomography Imaging in a Rabbit Model of Emphysema Reveals Ongoing Apoptosis *In Vivo*

Monica P. Goldklang[1,2], Yared Tekabe[2], Tina Zelonina[1], Jordis Trischler[1], Rui Xiao[1], Kyle Stearns[1], Alexander Romanov[3], Valeria Muzio[4], Takayuki Shiomi[1], Lynne L. Johnson[2]*, and Jeanine M. D'Armiento[1,2,5]*

[1]Department of Anesthesiology, [2]Department of Medicine, [3]Institute of Comparative Medicine, and [5]Department of Physiology and Cellular Biophysics, Columbia University Medical Center, New York, New York; and [4]Preclinical Pharmacology R&D, Advanced Accelerator Applications (Italy), Saint-Genis-Pouilly, Italy

Abstract

Evaluation of lung disease is limited by the inability to visualize ongoing pathological processes. Molecular imaging that targets cellular processes related to disease pathogenesis has the potential to assess disease activity over time to allow intervention before lung destruction. Because apoptosis is a critical component of lung damage in emphysema, a functional imaging approach was taken to determine if targeting apoptosis in a smoke exposure model would allow the quantification of early lung damage *in vivo*. Rabbits were exposed to cigarette smoke for 4 or 16 weeks and underwent single-photon emission computed tomography/computed tomography scanning using technetium-99m–rhAnnexin V-128. Imaging results were correlated with *ex vivo* tissue analysis to validate the presence of lung destruction and apoptosis. Lung computed tomography scans of long-term smoke–exposed rabbits exhibit anatomical similarities to human emphysema, with increased lung volumes compared with controls. Morphometry on lung tissue confirmed increased mean linear intercept and destructive index at 16 weeks of smoke exposure and compliance measurements documented physiological changes of emphysema. Tissue and lavage analysis displayed the hallmarks of smoke exposure, including increased tissue cellularity and protease activity. Technetium-99m–rhAnnexin V-128 single-photon emission computed tomography signal was increased after smoke exposure at 4 and 16 weeks, with confirmation of increased apoptosis through terminal deoxynucleotidyl transferase dUTP nick end labeling staining and increased tissue neutral sphingomyelinase activity in the tissue. These studies not only describe a novel emphysema model for use with future therapeutic applications, but, most importantly, also characterize a promising imaging modality that identifies ongoing destructive cellular processes within the lung.

Keywords: emphysema; smoke; apoptosis; molecular imaging

Current imaging modalities in lung disease primarily focus on the evaluation of organ damage and destruction (1). Although molecular imaging approaches have been established in oncology (2, 3) and in the assessment of cardiovascular disease (4), the utility of such an approach in nonneoplastic lung disease has not yet been established. The development of methods to image cellular processes and targets related to disease pathogenesis allows an evaluation over the time course of the

(Received in original form December 30, 2015; accepted in final form July 18, 2016)

*Co–senior authors.

This work was supported by National Institutes of Health (NIH) grants R01 HL116346 (J.M.D'A. and L.L.J.), R01 HL086936 (J.M.D'A.), and T32 HL007343 (M.P.G.). In addition, this work was funded by the Columbia University Irving Institute Clinical Trials Office Pilot Award, which is supported by the National Center for Advancing Translational Sciences, NIH, through grant UL1 TR000040. This work was also supported by the Center for Lymphangioleiomyomatosis and Rare Lung Diseases, Columbia University. Advanced Accelerator Applications in France provided the probe for imaging.

Author Contributions: Design of study and development of methodology (M.P.G., L.L.J., and J.M.D'A.), animal exposure (M.P.G., T.Z., and J.T.), animal imaging (M.P.G., Y.T., T.Z., J.T., A.R., V.M., and L.L.J.), animal sacrifice and tissue preservation (M.P.G., T.Z., J.T., and T.S.), data collection and analysis (M.P.G., Y.T., J.T., R.X., K.S., T.S., L.L.J., and J.M.D'A.), manuscript preparation (M.P.G., L.L.J., and J.M.D'A.).

Correspondence and requests for reprints should be addressed to Jeanine M. D'Armiento, M.D., Ph.D., Columbia University Medical Center, 630 West 168th Street, P&S 12-402, New York, NY 10032. E-mail: jmd12@cumc.columbia.edu

This article has an online supplement, which is accessible from this issue's table of contents at www.atsjournals.org

Am J Respir Cell Mol Biol Vol 55, Iss 6, pp 848–857, Dec 2016

Originally Published in Press as DOI: 10.1165/rcmb.2015-0407OC on August 2, 2016
Internet address: www.atsjournals.org

Clinical Relevance

Current pulmonary imaging modalities elucidate damaged and destroyed tissue but do not provide information regarding ongoing pathogenic processes. Here, we demonstrate a novel imaging modality that can identify, *in vivo*, apoptosis within the lungs of smoke-exposed animals correlating with disease activity. The rabbit smoke exposure model develops emphysema in a manner similar to the human disease, with apoptosis, increased protease activity, and characteristic morphometric and physiologic changes in the lung. *In vivo* technetium-99m–annexin V-128 imaging correlates with *ex vivo* tissue analyses of apoptosis, providing a novel imaging methodology that can aide with clinical prognostication and assessment of response to therapy in patients with chronic obstructive pulmonary disease.

disease, and provides information as a potential biomarker of disease activity and response to therapy.

Apoptosis is a process of programmed cell death that occurs during normal lung morphogenesis and development; however, apoptosis is uncommonly identified in the healthy adult lung (5). Apoptosis can be triggered by multiple stimuli that are pertinent in chronic obstructive pulmonary disease (COPD) pathogenesis, including loss of contact with the extracellular matrix, induction by immune cells, and various stressors, including oxidative stress (6, 7), and lung injury and repair (8, 9). Our group (10) and others (11) have established the presence of apoptosis in the human emphysematous lung with the level of apoptosis directly correlating with airway destruction in emphysema (10). Furthermore, a negative correlation has been established for apoptosis and lung surface area (10). There is a critical role for ceramide synthesis upstream of apoptosis (12), with neutral sphingomyelinase (nSMase) 2 activity elevated in the setting of cigarette smoke exposure (13). Elevated nSMase2 results in membrane–sphingomyelin hydrolysis and ceramide generation (13). As apoptosis continues in the setting of ongoing smoke exposure or additional insults, such as infection or disease exacerbations, without a compensatory proliferative response, lung destruction occurs. Despite the importance of apoptosis in the human disease state, smoke exposure in the mouse model of emphysema leads to variable levels of apoptosis within the lung (11, 14), in part due to differences in mouse genetic background. As a result, investigators have turned to alternative models of emphysema that more closely mimic the human disease (15–18).

Early in the process of apoptosis, phosphatidylserine (PS), which is normally confined to the inner sarcolemmal cell membrane layer, is transposed to the outer layer. Annexin V is a naturally occurring protein that binds PS. Labeling annexin V with a radioactive tracer has provided an important tool for diagnosing and quantifying apoptosis in live subjects. Hydrazinonicotinamide–annexin A5 (HYNIC-Anx), a technetium-99m (^{99m}Tc)–labeled imaging agent, has proven sensitive for detecting apoptosis in different diseases, including cancer and atherosclerosis (19–23). In this study, we used a direct ^{99m}Tc-labeled mutant of annexin (^{99m}Tc rhAnnexin V-128, herein referred to as AxV-128/Tc), which has improved binding affinity to PS, faster blood pool clearance, and similar biodistribution compared with ^{99m}Tc-HYNIC-Anx (14, 24).

Our initial studies establish the rabbit model of smoke exposure as a close mimic of the human disease with regard to inflammatory cell recruitment, protease induction, and emphysema development, including physiologic compliance changes. Subsequently, we used this model for investigating the novel apoptotic imaging agent. We hypothesized that uptake of AxV-128/Tc would be higher in the lungs of smoke-exposed rabbits compared with normal controls, and that quantitation of probe uptake would correlate with histopathology, providing a potential noninvasive marker to monitor disease activity and/or response to therapy in smoke-induced lung disease.

Materials and Methods

Animals

All animal studies were performed with the approval of the Institutional Animal Care and Use Committee of Columbia University (New York, NY). Female New Zealand white rabbits (weight, 1.3–1.8 kg) were obtained from Harlan Laboratories (Indianapolis, IN) and Charles River Laboratories (Wilmington, MA).

Exposure of Rabbits to Cigarette Smoke

Rabbits were acclimatized to the animal facility for at least 48 hours before use. Subsequently, animals underwent smoke exposure in a TE-10 Teague Smoking Apparatus (Teague Enterprises, Woodland, CA). University of Kentucky 3R4F Reference Cigarettes (University of Kentucky, Lexington, KY) were used and total particulate matter was maintained at 100–150 mg/m^3, as measured by gravimetric analysis. Rabbits underwent smoke exposure 4 hours per day, 5 days per week, for 4 or 16 weeks. Rabbits were always exposed to cigarette smoke the day before imaging and/or being killed. As a surrogate measure of smoke exposure, serum cotinine levels were determined by ELISA (Mouse/Rat Cotinine ELISA, SE120083; Sigma-Aldrich, St. Louis, MO), per the manufacturer's instructions.

Imaging Procedures

AxV-128/Tc was prepared by reconstitution of annexin V (provided by Advanced Accelerator Applications, Saint-Genis-Pouilly, France) with 18–22 mCi ^{99m}Tc in 2 ml volume. Rabbits were injected with 3.64 (±0.40) mCi AxV-128/Tc via an ear vein catheter. After 3 hours, rabbits were sedated with ketamine and xylazine and underwent single-photon emission computed tomography (SPECT) imaging on the nanoSPECT system (Mediso, Budapest, Hungary) fitted with two parallel hole collimators. Within 5 days of SPECT imaging, rabbits underwent a sedated spiral chest computed tomography (CT) on a Siemens 64 slice Biograph camera (Munich, Germany). After all SPECT and CT imaging, rabbits were killed, and fresh lung tissue was obtained for correlative gamma well counting. Gamma well counting was performed within 12 hours of radiotracer injection for SPECT imaging. For imaging analysis, SPECT and CT images were merged, reconstructed, and analyzed as outlined in the supplemental Materials and Methods. Organ biodistribution is also provided in the online supplement.

Lung Compliance Measurements

After killing with Euthasol (Virbac, Fort Worth, TX), a neck dissection was performed and a 3.5 endotracheal tube secured in the trachea with a suture. The end of the endotracheal tube was connected via three-way stopcock to a manometer and syringe for pressure measurements. The lung was sequentially inflated 5 ml at a time and pressure recorded after equilibration to a maximum volume of 25 ml (for 4-wk rabbits) or 40 ml (for 16-wk rabbits). These volumes are within 15–20% of the resting tidal volumes for smoke-exposed rabbits detected on CT scan.

Histologic and Morphometric Analysis

After the neck dissection, the chest was opened and dissected. Bronchoalveolar lavage (BAL) was performed, flushing 60 ml of sterile PBS into the lungs in two 30-ml increments. BAL fluid was spun for 10 minutes at 2,000 RPM, and supernatant removed and stored at −80°C for further analysis. The lungs were pressure inflated with 10% formalin to 25 cm H_2O. Each lung region (right upper, right lower, left upper, and left lower) was paraffin embedded, sectioned, and hematoxylin and eosin stained. At least 25 images at ×4 magnification were obtained per rabbit, with sampling performed in each lung region for morphometry, including mean linear intercept (14), a measure of airway enlargement, and destructive index (25), the percentage of the number of destroyed alveoli compared with the total number of alveoli. Tissue cell counts were performed on cell-specific immunohistochemistry sections. Lymphocytes were identified with anti-CD3 (ab11089, rat monoclonal to CD3 [CD3–12], 1:250; Abcam, Cambridge, MA). Macrophages were identified with anti-macrophage antibody (ab22506, mouse monoclonal to [MAC387] macrophage, 1:750; Abcam). Neutrophils were identified with anti-CD11b (MBS438151, rat monoclonal to CD11b [ITGAM], 1:10; MyBioSource, Inc., San Diego, CA). At least eight microscopic fields were randomly photographed and inflammatory cells per square millimeter were calculated for tissue cell counts (14).

Terminal Deoxynucleotidyl Transferase dUTP Nick End Labeling Staining

Terminal deoxynucleotidyl transferase dUTP nick end labeling (TUNEL) assay was performed on paraffin-embedded lung tissue sections (In Situ Cell Death Detection Kit, POD; Roche, Indianapolis, IN). At least five images were obtained at ×20 magnification. A ratio of TUNEL-positive to total nuclei was obtained to generate an apoptotic index.

Protease and Enzymatic Activity

Lung lysates were prepared from flash-frozen lung tissue. Lung protein concentration was assessed using the Pierce BCA Protein assay (Thermo Fisher, Grand Island, NY). Lung tissue cathepsin D activity (Abcam), BAL neutrophil elastase activity (Cayman Chemical, Ann Arbor, MI), and sphingomyelinase activity (Amplex Red Sphingomyelinase Assay Kit; Thermo Fisher) were measured per manufacturer directions. Gelatin zymography was performed (26, 27) to assess matrix metalloproteinase (MMP)-2 and MMP-9 activity.

Statistical Analysis

Uptake of AxV-128/Tc for each lung was averaged for each group (4-wk and 16-wk smoke and room air exposed) and groups compared using Student's *t* test. Similar comparisons were made between groups for morphometric analysis as well as the apoptotic index with *P* less than 0.05 considered statistically significant. Prism 6 for Mac OS X (GraphPad, San Diego, CA) was used for statistical analysis.

Results

Increased Airway Inflammation in the Smoke-Exposed Rabbit

As expected under smoke exposure conditions, the serum cotinine levels were significantly increased at both the 4-week (room air, 0.041 ± 0.26 ng/ml; smoke, 7.99 ± 6.03 ng/ml; $P = 0.028$) and 16-week

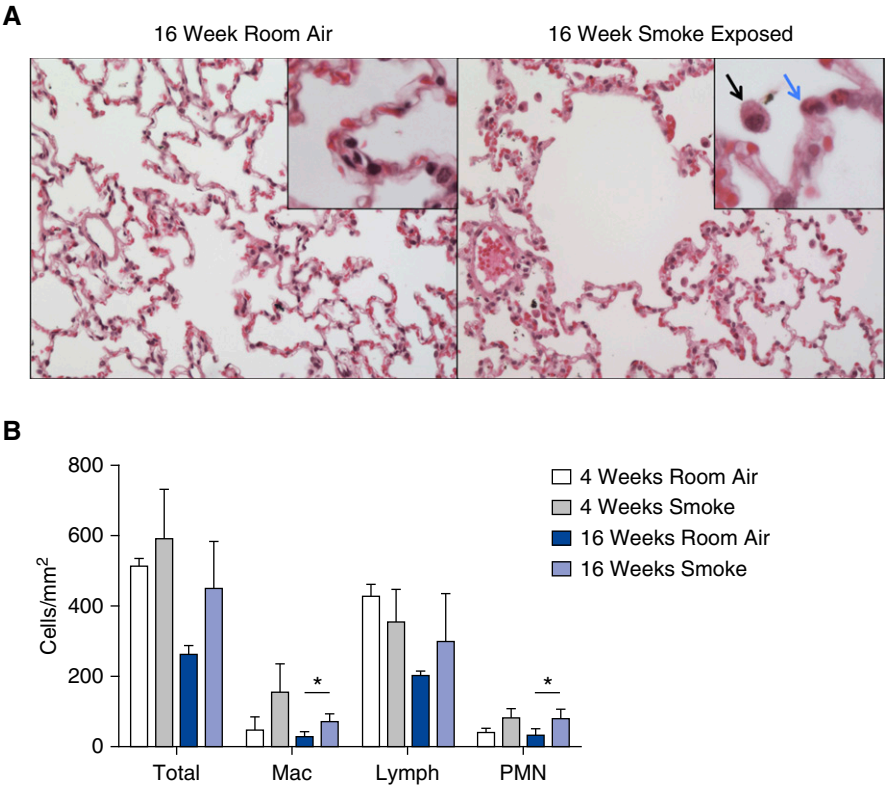

Figure 1. Increased tissue inflammatory cells in the smoke-exposed rabbit. (*A*) Increased inflammation in the lungs of 16-week smoke-exposed rabbits (*right panel*) as compared with room air control (*left panel*). The *black arrow* points to a macrophage and the *blue arrow* points to a neutrophil. *Main images* taken at ×20 magnification, and *inset images* were taken at ×40 magnification. (*B*) Total inflammatory cells (Total), macrophages (Mac), neutrophils (PMN), and lymphocytes (Lymph) in 4- and 16-week room air– and smoke-exposed rabbits ($n = 3$, 4-week room air; $n = 4$, 4-week smoke; $n = 3$, 16-week room air; $n = 6$, 16-week smoke). Increased neutrophils and macrophages were identified in 16-week smoke-exposure conditions. Data are presented as mean (±SD). *$P < 0.05$ versus room air control.

(room air, 0.49 ± 0.43 ng/ml; smoke, 75.23 ± 27.07 ng/ml; $P = 0.001$) time point of smoke exposure. Rabbits exhibit an increase in tissue cell counts within the lung (Figures 1A and 1B) after 16-weeks of smoke exposure, most notably in macrophages and neutrophils (Figure 1B).

Increased Protease Activity and Apoptosis in the Smoke-Exposed Rabbit Model

Initial studies demonstrated that MMP-1 protein expression is increased in the rabbit model after 8 weeks of exposure (27), consistent with what is seen in the human disease (28). Along with this increase in MMP-1 protein, there was a significant increase in BAL neutrophil elastase activity after 16 weeks of smoke exposure (Figure 2A), and after 4 weeks of smoke exposure there was an increase in cathepsin D activity in whole-lung homogenates (Figure 2B). Gelatin zymography demonstrated increased pro–MMP-9 and active MMP-9 at the 16-week smoke time point. There was an increase in pro–MMP-2 at the 16-week time point, but active MMP-2 was not present. MMP-2 was detected at low levels in all rabbit BAL fluid tested (Figure 2C).

Tissue from 4- and 16-week smoke-exposed rabbit lungs was examined for markers of cellular apoptosis. At both the 4- and 16-week time points, TUNEL staining revealed increased apoptosis in the lungs of smoke-exposed rabbits (Figure 3A). TUNEL-positive cells included pulmonary endothelial and epithelial cells, as well as macrophages (Figure 3A, *arrows*). Quantification confirms a statistically significant increase in TUNEL-positive cells at both 4 and 16 weeks of smoke exposure (Figure 3B).

nSMase synthesizes ceramide from membrane sphingomyelin in cells undergoing apoptosis, and is elevated in human emphysema and mouse models (29). The sphingomyelinase activity assay of whole-lung homogenates reveals a significant increase in nSMase activity under smoke exposure conditions (Figure 3C).

Radiographic Findings of Emphysema in the Smoke-Exposed Rabbit

Within 5 days of SPECT imaging, rabbits underwent spiral chest CT. Due to the predominant diaphragmatic breathing pattern of rabbits and a very short

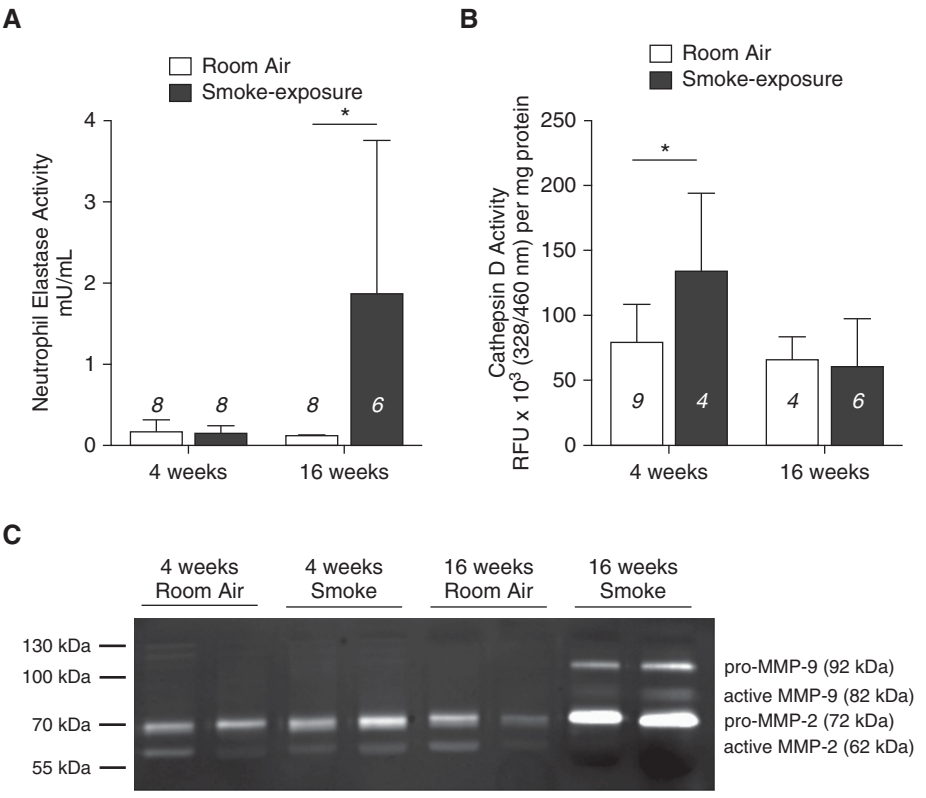

Figure 2. Increased protease activity after 4 weeks of smoke exposure. (*A*) Increased neutrophil elastase activity in the bronchoalveolar lavage (BAL) fluid of 16-week smoke-exposed rabbits ($P = 0.0204$, 16-week room air versus smoke-exposed). (*B*) Increased cathepsin D activity in whole-lung homogenates of 4-week smoke-exposed rabbits ($P = 0.0441$, 4-week room air versus smoke exposed). (*C*) Increased matrix metalloproteinase (MMP)-9 gelatinase activity in the BAL fluid of 16-week smoke-exposed rabbits. *$P < 0.05$ versus room air control. Data are presented as mean (±SD). RFU, relative fluorescence units.

acquisition time, scans exhibited only minimal or no blurring on the basal slices and, as such, respiratory gating was not performed. Representative midlung field transverse sections of a 16-week smoke-exposed and room air control rabbit are provided in Figure 4A. After image acquisition, serial transverse slices were summed into 1-cm-thick sections. Regions of interest were drawn around serial sections to calculate lung volumes and Hounsfield units (HU). As demonstrated in Figure 4B, there was a statistically significant increase in lung volume, as measured on chest CT, after 16 weeks of smoke exposure, with no difference seen at 4 weeks.

Although the mean value for HUs for the 16-week smoke-exposed rabbits was lower than for the 4-week smoke-exposed rabbits, there was not a statistically significant difference due to large standard deviations of values for both time periods for room air and smoke-exposed rabbits. However, when examining the segmental values for HUs, for the 16-week smoke-exposed rabbits, 10 of 20 segments revealed values below 2 SD of the mean for the 4-week room air–exposed rabbits, whereas, for the 16-week room air–exposed rabbits, there were only 2 of 24 segments with HU values below 2 SD of the mean for the 4-week room air–exposed rabbits.

Increased AxV-128/Tc Uptake in the Lungs of Smoke-Exposed Rabbits

AxV-128/Tc SPECT/CT imaging demonstrated increased uptake in the lungs of smoke-exposed rabbits at both the 4- and 16-week time points. Representative midlung field transverse reconstructed merged SPECT/CT images are shown in Figure 5A. Quantification of tracer uptake as percent injected dose (%ID) in both lungs was significantly higher in smoke-exposed rabbits compared with room air–exposed rabbits at both early (4 wk) and late (16 wk) time points, as shown in bar

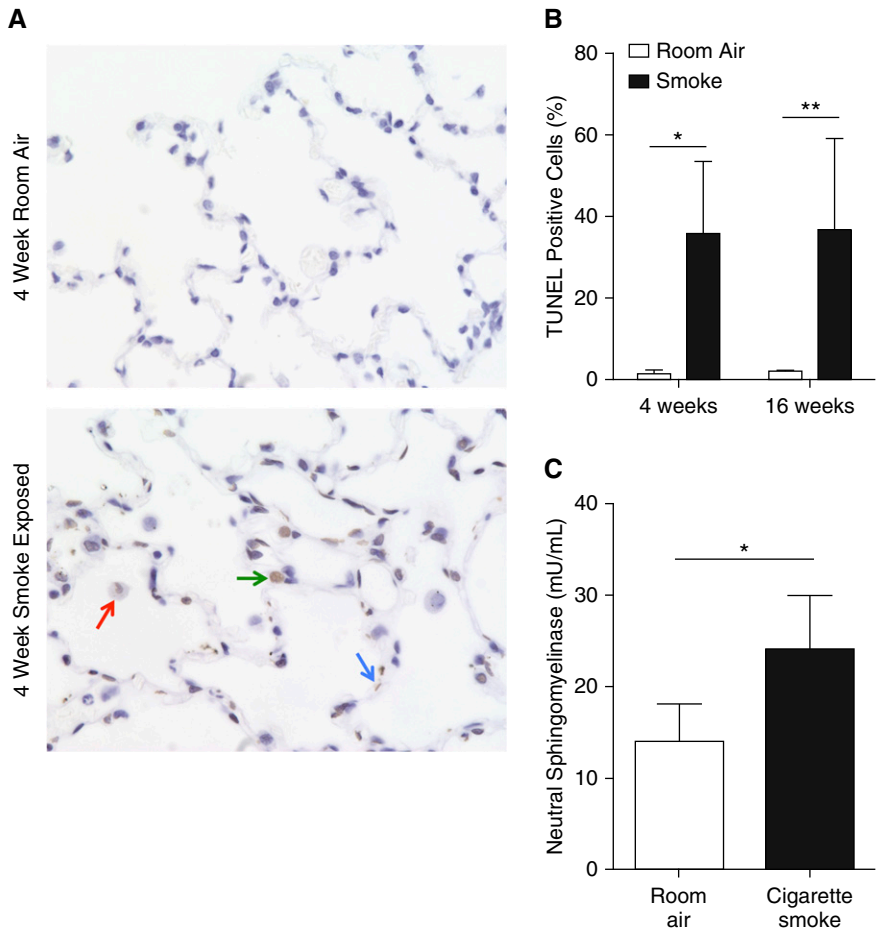

Figure 3. Increased markers of apoptosis in the lungs of smoke-exposed rabbits. (*A*) Representative images of increased terminal deoxynucleotidyl transferase dUTP nick end labeling (TUNEL)–positive cells after 4 weeks of smoke exposure. Images are taken at ×40 magnification. *Arrows* denote TUNEL-positive endothelial cells (*blue*), macrophages (*red*), and epithelial cells (*green*). (*B*) Quantification of TUNEL-positive cells ($n = 3$ per group; $P = 0.033$ 4-week room air versus smoke exposed, $P = 0.0093$ 16-week room air versus smoke exposed). (*C*) Increased neutral sphingomyelinase activity in the lung homogenates of 16-week smoke-exposed rabbits ($n = 5$ per group, $P = 0.0141$). $^{*}P < 0.05$ and $^{**}P < 0.01$ versus room air control. Data are presented as mean (±SD).

graphs in Figure 5B. After death, *ex vivo* gamma well counting obtained from tissue sections of the left upper, left lower, right upper, and right lower lobes confirmed increased radiotracer signal within the lungs of smoke-exposed rabbits (Figure 5C).

Airway Destruction and Increased Lung Compliance after Long-Term Smoke Exposure

To validate the imaging findings in smoke-exposed rabbits against physiologic and morphologic measures of emphysema found in the human disease, static lung compliance was assessed and standardized morphometry was performed on histologic samples. It was found that 4 weeks of smoke exposure leads to increased apoptosis, but there was no evidence of structural or physiologic changes consistent with emphysema at this early time point. However, after 16 weeks of smoke exposure, there was a statistically significant increase in static lung compliance (Figure 6A). In addition, at 16 weeks of smoke exposure, there was pathologic evidence of emphysema, with an increase in lung destruction, measured quantitatively using the mean linear intercept (Figure 6B) and destructive index (Figure 6C).

Discussion

In this study, the rabbit model of chronic smoke exposure is characterized and demonstrated to be pathologically similar to human COPD with regard to an increase in lung cellularity, protease activity, airway mechanic changes, airspace enlargement, and the development of cellular apoptosis. Furthermore, these studies successfully demonstrate that a probe targeting cells undergoing apoptosis has increased uptake in lungs of cigarette smoke–exposed rabbits, and can be imaged and semiquantified by SPECT/CT. The annexin V probe signal correlated with apoptosis demonstrated by TUNEL staining and increased neutral sphingomylinase activity in lung tissue removed at necropsy. This is the first report to apply molecular imaging targeting apoptosis to chronic lung disease in a relevant animal model.

The level of cigarette smoke exposure in this rabbit model of emphysema is in line with the exposures seen in human disease; serum cotinine levels from smoke-exposed rabbits fall within the lower end of the serum cotinine range documented in the self-identifying smokers in the National Health and Nutrition Examination Survey population (30). The proteolytic changes secondary to cigarette smoke seen in the rabbit model are documented to occur in the human disease (27, 31, 32) and in the mouse models (33–35). Cathepsin D is elevated in smoke exposure in both humans (36) and animal models (33), and we document in these studies the elevation of this protease in the rabbit smoke exposure model at an early time point. The discrepancy between the timing of smoke-induced increases in cathepsin D activity and neutrophil elastase activity likely reflects the alterations in inflammatory cell activation and the proteolytic response as the animal transitions from acute to chronic smoke exposure.

The mouse model of smoke-induced emphysema exhibits variable levels of infiltrating neutrophils depending on the mouse strain (37), and rarely exhibits neutrophil elastase activity in the BAL. The rabbit model presented in this study exhibits statistically significant increases in tissue neutrophils at 16 weeks of smoke exposure. This increase correlates with increased neutrophil elastase activity in BAL fluid. Interestingly, whereas at 4 weeks

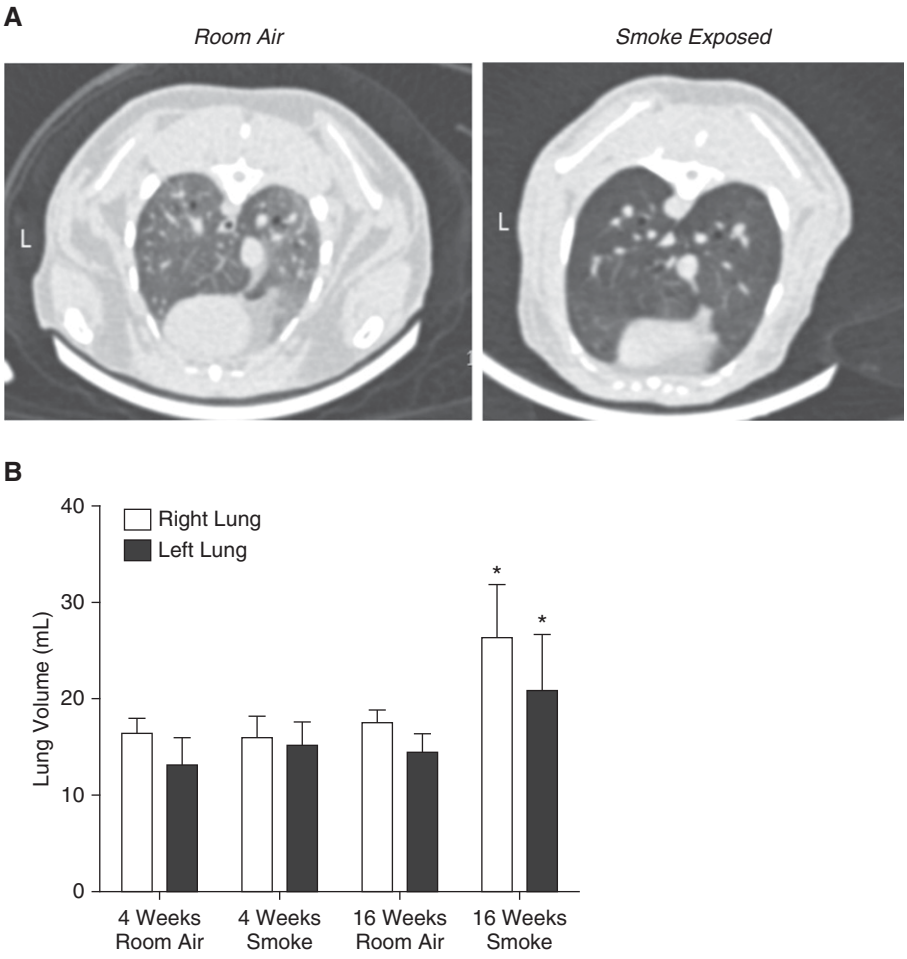

Figure 4. Lung computed tomography (CT) of smoke-exposed rabbits exhibits anatomical similarities to human emphysema, with larger lung volumes compared with room air controls. (*A*) Representative transverse CT sections from 16-week smoke-exposed and room air control rabbits. (*B*) Increased lung volumes in the 16-week smoke-exposed rabbit. Lung volumes calculated from 4-week room air ($n = 9$), 4-week smoke exposed ($n = 8$), 16-week room air ($n = 5$), and 16-week smoke exposed ($n = 4$). Data are presented as mean (±SD). *$P < 0.05$ versus ipsilateral side 4-week smoke exposure and 16-week room air control. L, left.

of smoke exposure there is a trend to increased tissue neutrophils, there is no alteration in neutrophil elastase activity. Work by Terashima and colleagues (38) details the effect of acute smoke exposure (11 d) on neutrophil sequestration; it is possible that the neutrophils identified in lung tissue at the 4-week time point are sequestered in the pulmonary microvessels, accounting for the trend to increased tissue neutrophils at this time point, but the lack of increase in neutrophil elastase activity in BAL fluid. The significant increase in neutrophil elastase activity upon long-term smoke exposure suggests that the rabbit model will be useful to test antielastolytic therapies in chronic smoke exposure models. Furthermore, the rabbit develops clear physiological changes representative of emphysema, which have not been demonstrated in all mouse models of smoke exposure (14). The development of the rabbit model will allow for the testing of matrix remodeling agents that could not be tested in the mouse.

Apoptosis or programmed cell death is an ordered process, with extrinsic receptor-mediated and intrinsic mitochondrial pathways, which activate a group of effector enzymes called caspases that cleave intracellular proteins (39). This process leads to typical morphological changes, including cell shrinking, chromatin condensation, nuclear fragmentation, and cell membrane changes. The latter includes the activation of a translocase that flips the bilayer lipid membrane and exposes the aminophospholipids, PS and phosphatidylethanolamine, from the inner to the outer cell surface, which then serve as "eat me" signals to phagocytes (39).

Annexin V is a 36-kD human protein, which serves as a naturally occurring anticoagulant and has a high affinity for PS. By linking annexin V with ^{99m}Tc via a chelator (^{99m}Tc-HYNIC-AnxV), a molecular imaging agent for SPECT imaging was developed and has been investigated as an *in vivo* marker for apoptotic cell death. Because apoptosis occurs in response to a number of stress signals and injury, including ischemia, oxidative stress, and toxins, it plays an important role in a wide spectrum of diseases (40). Preclinical and clinical trials of this probe have been investigated in subjects with myocardial ischemia and infarction (41, 42), in atherosclerosis (43, 44), and in cerebral ischemia (23, 45), and to follow the response of tumors to chemotherapeutic agents that induce cell death (46, 47). In our previous work, we have evaluated ^{99m}Tc-HYNIC-AnxV as a marker of macrophage cell death in atherosclerotic plaques in aortae of apolipoprotein E-null mice (48) and in the coronaries of hyperlipidemic pigs (43), and as a marker of the paracrine effects of conditioned stem cells to decrease myocyte cell death after cell engraftment into acutely ischemic myocardium (49).

Other approaches to probe development for apoptosis imaging have been pursued, including both new probes to target different steps in the process and to improve annexin V labeling. Approaches to target caspases have proven to be difficult due to the necessity of delivering the probe into the cells. Approaches to improve annexin V labeling include the development of annexin V mutants with endogenous chelation sites for ^{99m}Tc (50). Tait and coinvestigators (51) showed that all four domains of annexin V are required for optimal uptake in apoptotic tissues and, by adding an endogenous Tc chelation site to the N terminus of annexin V (annexin V-128), all four binding sites remain free. They also showed with an *in vitro* binding assay that binding site affinity is decreased by derivatization (52). These observations were born out by comparison of direct-labeled AxV-128/Tc with ^{99m}Tc-HYNIC-AnxV that

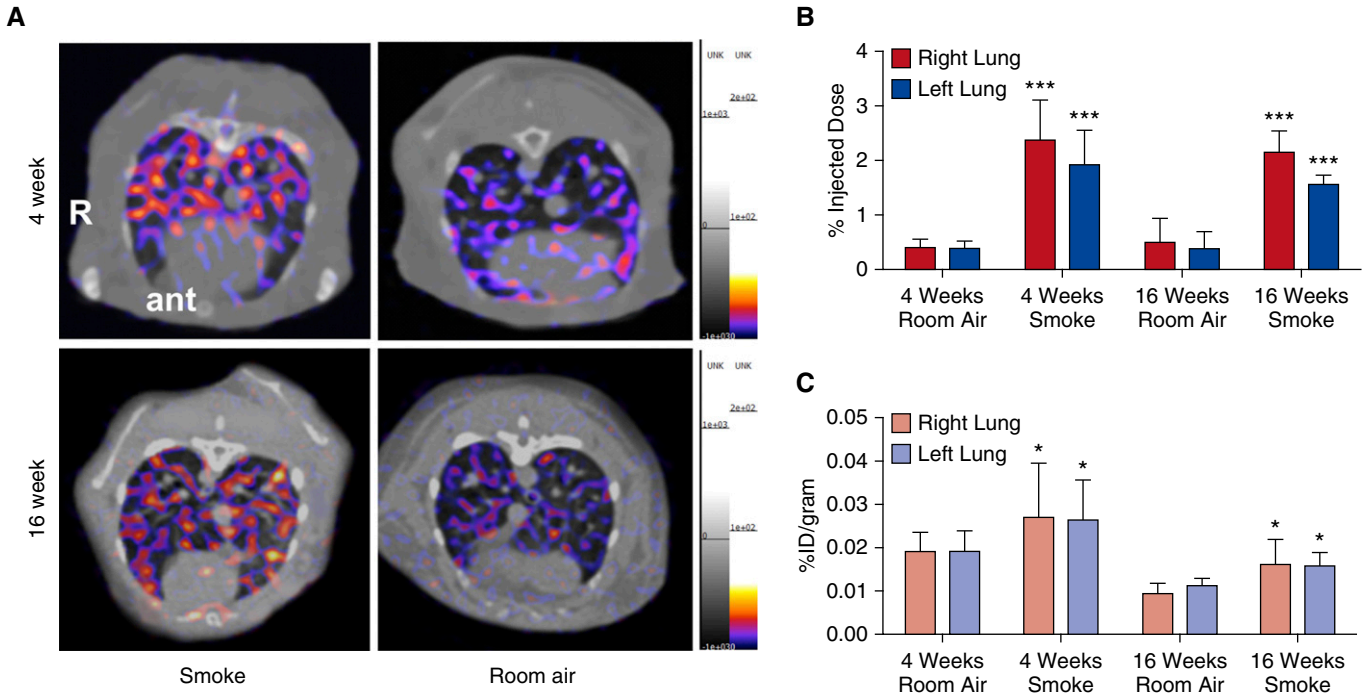

Figure 5. Increased apoptosis detected by AxV128/Tc single-photon emission CT (SPECT)/CT imaging in smoke exposure conditions. (*A*) Representative transverse midlung field SPECT/CT scans from smoke-exposed rabbits on *left*, room air on *right*, four week on *top*, 16 week on *bottom*. The lookup table *threshold bars* displayed *next to the figures* show the upper threshold levels chosen to display the lung uptake. R, right; ant, anterior. (*B*) AxV-128 SPECT imaging detected higher tracer uptake with smoke exposure at 4 weeks and at 16 weeks compared with room air. At 4 weeks, percent injected dose (%ID) for room air–exposed rabbits ($n = 6$) was 0.40 ± 0.16 for right lung (RL) and 0.39 ± 0.13 for left lung (LL), and, for smoke-exposed rabbits ($n = 6$), 2.37 ± 0.73 for RL and 1.92 ± 0.63 for LL ($P = 0.0009$ for RL, $P = 0.0016$ for LL). At 16 weeks of room air ($n = 5$), values were 0.50 ± 0.44 for RL and 0.38 ± 0.31 for LL, and, for smoke-exposed rabbits ($n = 5$), values were 2.14 ± 0.39 for RL and 1.56 ± 0.16 for LL ($P = 0.00025$ for RL, $P = 0.00028$ for LL). There was no significant difference in uptake for either lung between 4- and 16-week smoke exposure. (*C*) *Ex vivo* tissue analysis using gamma well counting, a measure of tissue radioactivity, confirmed these results. All data are presented as mean (±SD). ***$P < 0.001$ and *$P < 0.05$ as compared with ipsilateral room air control.

showed higher uptake of the direct-labeled probe in apoptotic tissue. In addition, there was lower dose to the kidneys with AxV-128/Tc. These properties support the superiority of AxV-128/Tc as an apoptosis imaging probe.

In the present study, we used AxV-128/Tc and documented lung uptake of the probe in smoke-exposed rabbits. This is the first reported application of apoptosis-targeted nuclear imaging in COPD using a relevant animal model. Importantly,

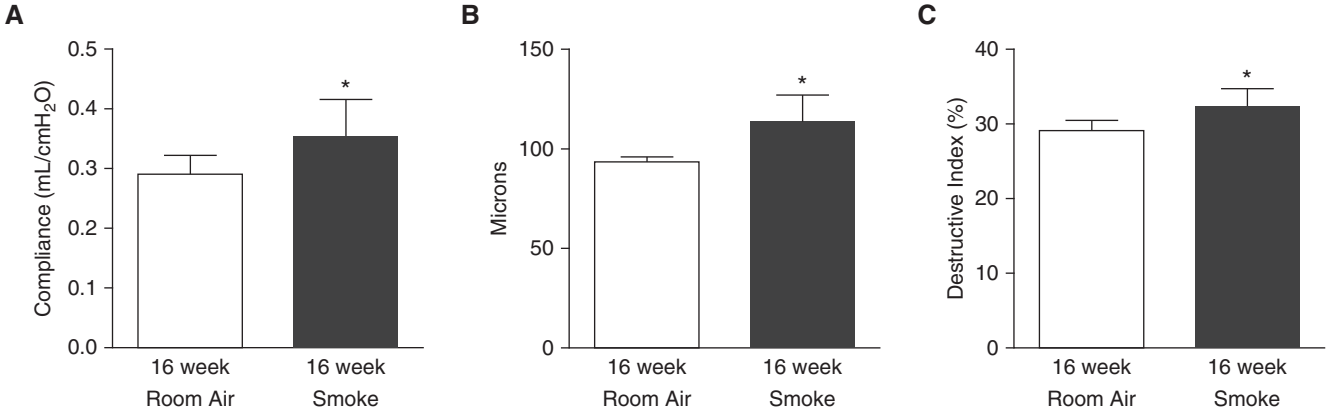

Figure 6. Physiologic and anatomic changes of emphysema in the rabbit smoke-exposure model. (*A*) Increased static lung compliance in the 16-week smoke-exposed rabbit ($n = 5$ room air, $n = 6$ smoke). (*B*) Increased mean linear intercept in 16-week smoke exposure ($n = 3$ room air, $n = 5$ smoke). (*C*) Increased destruction of alveoli, as measured by destructive index, in 16-week smoke exposure ($n = 3$ room air, $n = 5$ smoke). *$P < 0.05$ versus room air. Data are presented as mean (±SD). Changes were not significant at the 4-week smoke-exposure time point.

apoptosis was observed at 4 weeks of smoke exposure, a time point with no morphometric changes, demonstrating that AxV-128/Tc uptake does not change solely based on tissue destruction. To anatomically localize the signal from the marker molecule, hybrid SPECT/CT scanning is performed.

Although in the current study the CT scans were merged with the SPECT scans to define the lung boundaries and not perform segmental correlation, advantages of this hybrid imaging approach in patient studies would be to obtain more detailed assessment of regional differences in lung anatomy/pathology to correlate with regional differences in radiotracer uptake. Over time, as the inciting injury (cigarette smoke) continues, apoptosis may decrease as chronic injury causes a loss of lung tissue. Serial imaging in patients could, in theory, identify and possibly quantify areas of lung tissue actively undergoing apoptosis versus areas of normal lung tissue; such an approach could offer important additional information on disease stage to be used for clinical decision making. The choice of a positron emission tomography (PET)-labeled versus a SPECT-labeled radiotracer would depend on further development and clinical availability of PET-labeled probes for biological targets important in lung disease. Whether the improved sensitivity of PET versus SPECT is important for imaging small targets, SPECT/CT may be equally effective for imaging diffuse disease in an entire lung or lung segment. Both SPECT/CT and PET/CT cameras are widely available. The strength of the targeted approach described in this study is the availability of the radiotracer and the importance of the target, apoptosis, in development of COPD.

Although the rabbit model is ideal for the study of apoptosis and proteases under smoke exposure conditions, there are several limitations. The model is quite expensive; housing costs are up to 25 times higher than those of mice, and all mating of rabbits is performed with outside vendors rather than at a university. Furthermore, the rabbit genome is not fully sequenced, limiting the use of primers for genetic expression assays. In addition, many of the antibodies for tissue analysis (immunohistochemistry and Western blot) are not compatible with rabbit tissue.

In addition, because exposure of PS occurs early in the apoptotic process, it is possible that mitigation in the instigating stressor can stop and reverse the process. In this case, cells that bind the probe would eventually recover; therefore, quantifying the signal would overestimate the number of cells that ultimately die. This may occur in myocardial reperfusion injury with restoration of tissue oxygenation (53). Nevertheless, the extent of uptake of AxV-128/Tc signals severe cell injury and/or death and, in all the preclinical studies, including the present work, excellent correlations have been shown between probe uptake and TUNEL or quantitative caspase tissue staining by immunohistology.

The *in vivo* nuclear molecular imaging approach presented in this report is the first to apply this hybrid imaging technology to lung disease. There are several clinical issues facing patients with COPD that cannot be addressed with the standard modalities available for disease assessment. It is currently not possible to assess disease activity and predict which patients will develop disease progression after diagnosis, despite knowledge of the various critical pathogenic processes leading to lung destruction. In addition, the ability to monitor disease-targeted interventions is limited by the current clinical and imaging methodology available. The favorable results reported in this relevant rabbit animal model of smoke-induced lung disease potentially offers clinicians a tool to noninvasively image ongoing pathobiology in addition to destructive changes seen on CT scans. The hybrid nuclear/CT scanning modality is widely available, and the techniques presented are easily translatable to human patients for testing to determine if the assessment of ongoing pathobiological changes can predict prognosis and follow therapeutic response. ■

Author disclosures are available with the text of this article at www.atsjournals.org.

Acknowledgments: The authors thank Tomoe Shiomi (Columbia University, New York, NY) for her help with histology and Tamykah Anthony (Columbia University, New York, NY) for her assistance with rabbit imaging; V.M. works for Advanced Accelerator Applications in France and provided the probe for imaging.

References

1. Washko GR. Diagnostic imaging in COPD. *Semin Respir Crit Care Med* 2010;31:276–285.
2. Everitt S, Hicks RJ, Ball D, Kron T, Schneider-Kolsky M, Walter T, Binns D, Mac Manus M. Imaging cellular proliferation during chemo-radiotherapy: a pilot study of serial 18F-FLT positron emission tomography/computed tomography imaging for non–small-cell lung cancer. *Int J Radiat Oncol Biol Phys* 2009;75: 1098–1104.
3. Rischin D, Hicks RJ, Fisher R, Binns D, Corry J, Porceddu S, Peters LJ; Trans-Tasman Radiation Oncology Group Study 98.02. Prognostic significance of [18F]-misonidazole positron emission tomography–detected tumor hypoxia in patients with advanced head and neck cancer randomly assigned to chemoradiation with or without tirapazamine: a substudy of Trans-Tasman Radiation Oncology Group Study 98.02. *J Clin Oncol* 2006;24: 2098–2104.
4. Nahrendorf M, Frantz S, Swirski FK, Mulder WJ, Randolph G, Ertl G, Ntziachristos V, Piek JJ, Stroes ES, Schwaiger M, *et al*. Imaging systemic inflammatory networks in ischemic heart disease. *J Am Coll Cardiol* 2015;65:1583–1591.
5. Mercer BA, Lemaître V, Powell CA, D'Armiento J. The epithelial cell in lung health and emphysema pathogenesis. *Curr Respir Med Rev* 2006;2:101–142.
6. Morissette MC, Parent J, Milot J. Alveolar epithelial and endothelial cell apoptosis in emphysema: what we know and what we need to know. *Int J Chron Obstruct Pulmon Dis* 2009;4:19–31.
7. Martin TR, Nakamura M, Matute-Bello G. The role of apoptosis in acute lung injury. *Crit Care Med* 2003;31(4 suppl): S184–S188.
8. Herold S, Ludwig S, Pleschka S, Wolff T. Apoptosis signaling in influenza virus propagation, innate host defense, and lung injury. *J Leukoc Biol* 2012;92:75–82.
9. Drakopanagiotakis F, Xifteri A, Polychronopoulos V, Bouros D. Apoptosis in lung injury and fibrosis. *Eur Respir J* 2008;32: 1631–1638.
10. Imai K, Mercer BA, Schulman LL, Sonett JR, D'Armiento JM. Correlation of lung surface area to apoptosis and proliferation in human emphysema. *Eur Respir J* 2005;25:250–258.
11. Sakao S, Tatsumi K, Hashimoto T, Igari H, Shino Y, Shirasawa H, Kuriyama T. Vascular endothelial growth factor and the risk of smoking-related COPD. *Chest* 2003;124: 323–327.

12. Petrache I, Natarajan V, Zhen L, Medler TR, Richter AT, Cho C, Hubbard WC, Berdyshev EV, Tuder RM. Ceramide upregulation causes pulmonary cell apoptosis and emphysema-like disease in mice. *Nat Med* 2005;11:491–498.
13. Levy M, Khan E, Careaga M, Goldkorn T. Neutral sphingomyelinase 2 is activated by cigarette smoke to augment ceramide-induced apoptosis in lung cell death. *Am J Physiol Lung Cell Mol Physiol* 2009;297:L125–L133.
14. Foronjy RF, Mercer BA, Maxfield MW, Powell CA, D'Armiento J, Okada Y. Structural emphysema does not correlate with lung compliance: lessons from the mouse smoking model. *Exp Lung Res* 2005;31:547–562.
15. Goldklang MP, Marks SM, D'Armiento JM. Second hand smoke and COPD: lessons from animal studies. *Front Physiol* 2013;4:30.
16. Polverino F, Doyle-Eisele M, McDonald J, Wilder JA, Royer C, Laucho-Contreras M, Kelly EM, Divo M, Pinto-Plata V, Mauderly J, *et al*. A novel nonhuman primate model of cigarette smoke–induced airway disease. *Am J Pathol* 2015;185:741–755.
17. Kim Y, Chongviriyaphan N, Liu C, Russell RM, Wang XD. Combined α-tocopherol and ascorbic acid protects against smoke-induced lung squamous metaplasia in ferrets. *Lung Cancer* 2012;75:15–23.
18. Golovatch P, Mercer BA, Lemaître V, Wallace A, Foronjy RF, D'Armiento J. Role for cathepsin K in emphysema in smoke-exposed guinea pigs. *Exp Lung Res* 2009;35:631–645.
19. Kartachova MS, Valdés Olmos RA, Haas RL, Hoebers FJ, van Herk M, Verheij M. 99mTc-HYNIC-rh–annexin-V scintigraphy: visual and quantitative evaluation of early treatment-induced apoptosis to predict treatment outcome. *Nucl Med Commun* 2008; 29:39–44.
20. Hoebers FJ, Kartachova M, de Bois J, van den Brekel MW, van Tinteren H, van Herk M, Rasch CR, Valdés Olmos RA, Verheij M. 99mTc Hynic-rh–annexin V scintigraphy for *in vivo* imaging of apoptosis in patients with head and neck cancer treated with chemoradiotherapy. *Eur J Nucl Med Mol Imaging* 2008;35:509–518.
21. Rottey S, Slegers G, Van Belle S, Goethals I, Van de Wiele C. Sequential 99mTc-hydrazinonicotinamide–annexin V imaging for predicting response to chemotherapy. *J Nucl Med* 2006;47: 1813–1818.
22. Lorberboym M, Blankenberg FG, Sadeh M, Lampl Y. *In vivo* imaging of apoptosis in patients with acute stroke: correlation with blood–brain barrier permeability. *Brain Res* 2006;1103:13–19.
23. Blankenberg FG, Kalinyak J, Liu L, Koike M, Cheng D, Goris ML, Green A, Vanderheyden JL, Tong DC, Yenari MA. 99mTc-HYNIC–annexin V SPECT imaging of acute stroke and its response to neuroprotective therapy with anti-Fas ligand antibody. *Eur J Nucl Med Mol Imaging* 2006;33:566–574.
24. Benali K, Louedec L, Azzouna RB, Merceron O, Nassar P, Al Shoukr F, Petiet A, Barbato D, Michel JB, Sarda-Mantel L, *et al*. Preclinical validation of 99mTc–annexin A5-128 in experimental autoimmune myocarditis and infective endocarditis: comparison with 99mTc-HYNIC–annexin A5. *Mol Imaging* 2014;13:1–10.
25. Saetta M, Shiner RJ, Angus GE, Kim WD, Wang NS, King M, Ghezzo H, Cosio MG. Destructive index: a measurement of lung parenchymal destruction in smokers. *Am Rev Respir Dis* 1985;131: 764–769.
26. Heussen C, Dowdle EB. Electrophoretic analysis of plasminogen activators in polyacrylamide gels containing sodium dodecyl sulfate and copolymerized substrates. *Anal Biochem* 1980;102: 196–202.
27. Geraghty P, Dabo AJ, D'Armiento J. TLR4 protein contributes to cigarette smoke–induced matrix metalloproteinase-1 (MMP-1) expression in chronic obstructive pulmonary disease. *J Biol Chem* 2011;286:30211–30218.
28. Imai K, Dalal SS, Chen ES, Downey R, Schulman LL, Ginsburg M, D'Armiento J. Human collagenase (matrix metalloproteinase-1) expression in the lungs of patients with emphysema. *Am J Respir Crit Care Med* 2001;163:786–791.
29. Filosto S, Castillo S, Danielson A, Franzi L, Khan E, Kenyon N, Last J, Pinkerton K, Tuder R, Goldkorn T. Neutral sphingomyelinase 2: a novel target in cigarette smoke–induced apoptosis and lung injury. *Am J Respir Cell Mol Biol* 2011;44:350–360.
30. Benowitz NL, Bernert JT, Caraballo RS, Holiday DB, Wang J. Optimal serum cotinine levels for distinguishing cigarette smokers and nonsmokers within different racial/ethnic groups in the United States between 1999 and 2004. *Am J Epidemiol* 2009;169: 236–248.
31. Almansa R, Socias L, Sanchez-Garcia M, Martín-Loeches I, del Olmo M, Andaluz-Ojeda D, Bobillo F, Rico L, Herrero A, Roig V, *et al*. Critical COPD respiratory illness is linked to increased transcriptomic activity of neutrophil proteases genes. *BMC Res Notes* 2012;5:401.
32. Damiano VV, Tsang A, Kucich U, Abrams WR, Rosenbloom J, Kimbel P, Fallahnejad M, Weinbaum G. Immunolocalization of elastase in human emphysematous lungs. *J Clin Invest* 1986;78: 482–493.
33. Bracke K, Cataldo D, Maes T, Gueders M, Noël A, Foidart JM, Brusselle G, Pauwels RA. Matrix metalloproteinase-12 and cathepsin D expression in pulmonary macrophages and dendritic cells of cigarette smoke–exposed mice. *Int Arch Allergy Immunol* 2005; 138:169–179.
34. Shapiro SD, Goldstein NM, Houghton AM, Kobayashi DK, Kelley D, Belaaouaj A. Neutrophil elastase contributes to cigarette smoke–induced emphysema in mice. *Am J Pathol* 2003;163: 2329–2335.
35. Guyot N, Wartelle J, Malleret L, Todorov AA, Devouassoux G, Pacheco Y, Jenne DE, Belaaouaj A. Unopposed cathepsin G, neutrophil elastase, and proteinase 3 cause severe lung damage and emphysema. *Am J Pathol* 2014;184:2197–2210.
36. Chang JC, Yoo OH, Lesser M. Cathepsin D activity is increased in alveolar macrophages and bronchoalveolar lavage fluid of smokers. *Am Rev Respir Dis* 1989;140:958–960.
37. Pouwels SD, Heijink IH, Brouwer U, Gras R, den Boef LE, Boezen HM, Korstanje R, van Oosterhout AJ, Nawijn MC. Genetic variation associates with susceptibility for cigarette smoke-induced neutrophilia in mice. *Am J Physiol Lung Cell Mol Physiol* 2015;308: L693–L709.
38. Terashima T, Klut ME, English D, Hards J, Hogg JC, van Eeden SF. Cigarette smoking causes sequestration of polymorphonuclear leukocytes released from the bone marrow in lung microvessels. *Am J Respir Cell Mol Biol* 1999;20:171–177.
39. De Saint-Hubert M, Prinsen K, Mortelmans L, Verbruggen A, Mottaghy FM. Molecular imaging of cell death. *Methods* 2009;48: 178–187.
40. Favaloro B, Allocati N, Graziano V, Di Ilio C, De Laurenzi V. Role of apoptosis in disease. *Aging (Albany, NY)* 2012;4:330–349.
41. Hofstra L, Liem IH, Dumont EA, Boersma HH, van Heerde WL, Doevendans PA, De Muinck E, Wellens HJ, Kemerink GJ, Reutelingsperger CP, *et al*. Visualisation of cell death *in vivo* in patients with acute myocardial infarction. *Lancet* 2000;356: 209–212.
42. Thimister PW, Hofstra L, Liem IH, Boersma HH, Kemerink G, Reutelingsperger CP, Heidendal GA. *In vivo* detection of cell death in the area at risk in acute myocardial infarction. *J Nucl Med* 2003;44: 391–396.
43. Johnson LL, Schofield L, Donahay T, Narula N, Narula J. 99mTc–annexin V imaging for *in vivo* detection of atherosclerotic lesions in porcine coronary arteries. *J Nucl Med* 2005;46: 1186–1193.
44. Cheng D, Li X, Zhang C, Tan H, Wang C, Pang L, Shi H. Detection of vulnerable atherosclerosis plaques with a dual-modal single-photon-emission computed tomography/magnetic resonance imaging probe targeting apoptotic macrophages. *ACS Appl Mater Interfaces* 2015; 7:2847–2855.
45. Mari C, Karabiyikoglu M, Goris ML, Tait JF, Yenari MA, Blankenberg FG. Detection of focal hypoxic–ischemic injury and neuronal stress in a rodent model of unilateral MCA occlusion/reperfusion using radiolabeled annexin V. *Eur J Nucl Med Mol Imaging* 2004;31: 733–739.
46. Kurihara H, Yang DJ, Cristofanilli M, Erwin WD, Yu DF, Kohanim S, Mendez R, Kim EE. Imaging and dosimetry of 99mTc EC annexin V: preliminary clinical study targeting apoptosis in breast tumors. *Appl Radiat Isot* 2008;66:1175–1182.

47. Kartachova M, van Zandwijk N, Burgers S, van Tinteren H, Verheij M, Valdés Olmos RA. Prognostic significance of 99mTc Hynic-rh–annexin V scintigraphy during platinum-based chemotherapy in advanced lung cancer. *J Clin Oncol* 2007;25:2534–2539.
48. Tekabe Y, Li Q, Luma J, Weisenberger D, Sedlar M, Harja E, Narula J, Johnson LL. Noninvasive monitoring the biology of atherosclerotic plaque development with radiolabeled annexin V and matrix metalloproteinase inhibitor in spontaneous atherosclerotic mice. *J Nucl Cardiol* 2010;17:1073–1081.
49. Godier-Furnémont AF, Tekabe Y, Kollaros M, Eng G, Morales A, Vunjak-Novakovic G, Johnson LL. Noninvasive imaging of myocyte apoptosis following application of a stem cell–engineered delivery platform to acutely infarcted myocardium. *J Nucl Med* 2013;54: 977–983.
50. Tait JF, Brown DS, Gibson DF, Blankenberg FG, Strauss HW. Development and characterization of annexin V mutants with endogenous chelation sites for (99m)Tc. *Bioconjug Chem* 2000;11: 918–925.
51. Tait JF, Smith C, Levashova Z, Patel B, Blankenberg FG, Vanderheyden JL. Improved detection of cell death *in vivo* with annexin V radiolabeled by site-specific methods. *J Nucl Med* 2006;47: 1546–1553.
52. Tait JF, Smith C, Blankenberg FG. Structural requirements for *in vivo* detection of cell death with 99mTc–annexin V. *J Nucl Med* 2005;46: 807–815.
53. Strauss HW, Narula J, Blankenberg FG. Radioimaging to identify myocardial cell death and probably injury. *Lancet* 2000;356: 180–181.